Sustainable Battery Components from Biomass-Derived Lignin and Cellulose Extracted Using Deep Eutectic Solvents

Akiko Tsurumaki[1,2,*], Luca Stefanuto[3], Valentina Liberti[1], Corrado Zamparelli[1], Alessandra Gentili[1,2], Tecla Gasperi[3,4], and Maria Assunta Navarra[1,2]

[1]*Department of Chemistry, Sapienza University of Rome, Piazzale Aldo Moro 5, 00185, Rome Italy*

[2]*Hydro-Eco Research Center, Sapienza University of Rome, Via A. Scarpa 16, 00161, Rome Italy*

[3]*Department of Science, Roma Tre University, Viale Guglielmo Marconi 446, Rome Italy*

[4] *Laboratory of Nanomaterials for Environment and Health (NAMES), Biostructures and Biosystems National Institute (INBB), via dei Carpegna 19, Rome, Italy*

**Corresponding Author: Akiko Tsurumaki (akiko.tsurumaki@uniroma1.it)*

Abstract

Toward a more sustainable energy storage system, greener battery components were developed using lignin (LSE) and cellulose (CP), extracted from poplar wood and pistachio shells, respectively. Deep eutectic solvents (DESs) were employed as eco-friendly extraction media for the extraction of CP, owing to their low toxicity, simple preparation, recyclability, and cost-effectiveness, while a traditional steam explosion method was used for LSE extraction. The extracted LSE was used to synthesize hard carbon anode material, delivering stable capacity values exceeding 330 mAh g^{-1} over 200 cycles. On the other hand, CP was evaluated as a binder substituting sodium carboxymethyl cellulose (CMC) in aqueous $LiNi_{0.5}Mn_{1.5}O_4$ (LNMO)-based cathode slurries. Electrochemical performance in Li-metal cells demonstrated that CP provided enhanced long-term cycling stability, while CMC showed superior rate capability.

Keyword

Cellulose, Lignin, Biomass, Lithium-ion battery, Greener materials

Introduction

The transition away from fossil fuels for electric power generation systems is a critical step toward the goals outlined in 'The European Green Deal', which aims for net-zero greenhouse gas emissions by 2050 [1,2]. Alkali-metal or alkali-ion batteries such as Li-metal batteries (LMBs) and Li-ion batteries (LIBs) represent the state-of-the-art energy storage technologies owing to their high energy densities. These battery performances are typically evaluated using several key metrics, including specific energy (Wh kg^{-1}), energy density (Wh L^{-1}), specific power (W kg^{-1}), power density (W L^{-1}), safety, cycle life, calendar life, and charging time (i.e., fast charging ability) [3]. More recently, considerations of cost and environmental sustainability are becoming essential for progressing toward a more sustainable energy future [4,5].

At the stage of material synthesis, the development of more sustainable LIBs requires prioritizing raw-material accessibility, synthesis simplicity, and ease of material handling. Several commonly used battery components, such as cobalt, fluorspar, lithium, magnesium, and natural graphite, are classified as critical raw materials (CRMs) that are economically indispensable but are at risk of supply disruption and depletion [6]. The use of naturally occurring materials offers a promising strategy to reduce both environmental impact and geopolitical supply risks. Among them, biomasses composed of cellulose, hemicellulose, and lignin, have garnered significant attention as an abundant and renewable feedstock. The direct utilization of biomass-derived materials, if feasible, could contribute to minimizing energy consumption, chemical waste, and production costs, thereby contributing to more sustainable and scalable battery technologies.

In the field of batteries, cellulose derivatives, most notably sodium carboxymethyl cellulose (CMC), are commonly used as binders for electrodes or separators [7,8], together with other bio-derived polymers such as guar gum, chitosan, and alginate [9]. The use of these binders in electrode formulations enables the use of water to prepare electrode slurries, effectively replacing harmful organic solvents such as *N*-methyl pyrrolidone (NMP) [10]. This shift not only lowers production costs but also significantly reduces environmental footprint, paving the way for greener and safer battery manufacturing [11]. However, aqueous processing poses challenges for high-voltage cathode due to lithium leaching and concurrent pH increase, which lead to corrosion of aluminum current collectors. To mitigate these issues, recent strategies have focused on pH adjustment using mild acids (e.g., citric acid, acetic acid, phosphoric acid, poly(acrylic acid)) [12] or CO_2 [13], alongside the formation of protective coatings on active material particles or aluminum foil [14].

In contrast, lignin is primarily recognized as a carbon-rich feedstock and is mainly utilized as a precursor for carbon materials in battery applications [7,15]. The properties of biomass-derived carbon materials vary depending on the chemical composition of the precursor, the pre-treatment and activation methods, and the carbonization temperature and atmosphere. Among these, hard carbon (HC) is one of the promising anode materials due to its disordered and porous structure, providing additional site for lithium intercalation [16]. The pyrolysis temperature is a critical factor in determining the crystalline structure of the resulting material, with lower temperatures favoring the formation of amorphous HC and higher temperatures promoting the development of crystalline, graphite-like carbons [17,18]. In addition, hydrothermal treatment with acids can

significantly increase the surface area and porosity of HC, therefore improving metal-ion diffusion and storage capacity. [19,20].

Regarding biomass treatment, a wide range of methods has been developed to efficiently fractionate biomass into its main components, i.e., cellulose, hemicellulose, and lignin, and to enable their subsequent recycling and valorization, such as steam explosion, dilute acid treatment, alkaline treatment, Kraft pulping, and organosolv treatments [21,22]. Despite their widespread use, these conventional pretreatment technologies have several limitations such as energy consumption related to high temperature and high pressure treatments, degradation of the monosaccharides into other byproducts, and corrosion of equipment related to the use of acid. For example, in the steam explosion method, biomass is heated to 160–260 °C under high pressure (7–50 bar), followed by rapid depressurization that disrupts the cell structure. Dilute acid pretreatment is typically conducted with sulfuric acid (<5 wt%) at relatively high temperatures (120–160 °C). Recently, deep eutectic solvents (DESs), including low transition temperature mixtures (LTTMs) in the broad sense, are recognized as a novel class of solvents for biomass processing. They are engineered through the complexation of Lewis or Brønsted acids and bases [23,24]. More specifically, they typically formed by the complexation of a quaternary ammonium salt acting as a hydrogen bond acceptor (HBA) with a metal salt or hydrogen bond donor (HBD), such as phenolic derivatives. These solvents possess a unique set of properties that make them promising alternatives to conventional organic solvents, such as negligible vapor pressure, non-flammability, a wide liquid-phase temperature range, high thermal and chemical stability, moisture tolerance, environmental friendliness,

and easy biodegradability [25]. Their tunable composition allows for designed interaction with biomass components like lignin and cellulose, offering a selective and efficient pretreatment strategy.

In this study, the extraction of cellulose and lignin from biomass using LTTMs was developed as a preliminary step toward the sustainable production of materials for LIBs. LTTMs were selected due to their more sustainable characteristics compared to conventional solvents [26] and their effective ability to disrupt the strong hydrogen bonding networks within lignocellulosic matrices [27–29]. To enhance extraction efficiency and preserve the structural integrity of the extracted materials, while avoiding undesirable side reactions such as hydroxylation, demethoxylation, condensation, and crosslinking formation [30], both the dissolution and precipitation procedures were optimized based on methodologies reported in the literature [31–33]. The resulting materials, along with lignin extracted via the conventional steam explosion method, were then utilized in the development of battery components. This work addresses sustainability comprehensively by applying green principles both in developing battery components and in extracting biomass, thereby establishing an integrated system aligned with the goals of sustainable energy storage system.

Experimental section

Materials

Components of DES were purchased from Sigma Aldrich and utilized without further purification, such as resorcinol (99%), 4-methoxyphenonl (98%), 2-methoxyphenonl (99%), pyrogallol (98%), and choline chloride (ChCl, 98%) which was dried before use. For electrode preparation, commercially available $LiNi_{0.5}Mn_{1.5}O_4$

(LNMO, from NEI Corporation), Super-P conductive carbon (SP, from Timcal), poly(vinylidene fluoride) Solef® 6020 (PVdF, from Solvay), and sodium carboxymethyl cellulose Mw ~700,000 (CMC, from Merck KGaA) were used. Prepared electrodes were examined using an electrolyte, namely 1 M $LiPF_6$ in ethylene carbonate - dimethyl carbonate 1:1 v/v (LP30, from Merck KGaA).

Preparation of DES

DESs were synthesized by mixing ChCl with either resorcinol, 4-methoxyphenol, 2-methoxyphenol, or pyrogallol in precisely defined stoichiometric ratios, each in a separate preparation. Each binary mixture was heated at 80 °C under stirring until a visually transparent, homogeneous liquid was achieved. The molar ratios employed were as follows: ChCl : resorcinol 1:2, ChCl : 4-methoxyphenol 1:2, ChCl : 2-methoxyphenol 1:2, and ChCl : pyrogallol 1:1.

Extraction of biomass

Extraction of cellulose (CP) and lignin (LP) from pistachio shells was carried out as follows. To 2 g of the freshly prepared DES, 100 μL of H_3PO_4 aq. (85% v/v, diluted tenfold with deionized water) was added under stirring until a homogeneous mixture was obtained. Subsequently, 200 mg of fine powders from pistachio shells were added to the mixture and stirred at 100 °C for 72 hours. After mixing, a 1 M aqueous solution of NaOH was added dropwise to precipice biomass, primarily composed of cellulose, which was then collected by centrifugation at 5000 rpm for 5 minutes. A total of 120 mg of CP powder was obtained and washed three times

with 1 M NaOH, with gentle heating at 50 °C for 20 minutes, if necessary to facilitate dispersion. In contrast, the supernatant was neutralized by the addition of 1 M HCl and then diluted with chilled water (4 °C) to induce lignin precipitation, which was recovered by vacuum filtration, washed thoroughly with chilled water, and dried, yielding 60 mg of LP. Since the amount of obtained LP was insufficient for material development, lignin (LSE) was additionally extracted from poplar wood using the traditional steam explosion method [34]. The LSE was provided by the Trisaia Research Centre, Italian National Agency for New Technologies, Energy and Sustainable Economic Development (ENEA).

Preparation of electrodes with hard carbon

By using LSE, HC was synthesized according to the literature [35]. LSE, milli-Q water (18.2 MΩ cm^{-1} at 25 °C), and citric acid were mixed in a ratio of 8:20:0.1 in wt% and placed in a Teflon lined autoclave reactor, which was treated at 250 °C for 7.5 h to obtain hydrochar. After vacuum filtration of the obtained material to remove residual acid, it was pre-dried in an oven and then treated in a tube furnace at 600 °C for 2 hours with a heating ratio of 10 °C min^{-1}, in Ar flow. To evaluate the effect of impurities resulting from the extraction procedure, the purification was performed three times after HC synthesis by mixing it with Milli-Q water, sonicating for 5 min, and separating it with a centrifuge.

The obtained HCs with and without purification were utilized as an active material of LIBs. Slurries containing 80wt% dried HC, 10wt% SP, and 10wt% binder (either PVdF or CMC) were prepared using N-methylpyrrolidone or Milli-Q water as a solvent, which were applied on copper foils by using a doctor-blade.

The sheets were dried at 60 °C and cut into 1cm diameter disks. The cut electrodes were dried under vacuum at 120 °C for overnight.

Preparation of LNMO electrodes

CP was purified in a similar manner for HC prior to its use. Electrode slurries were prepared by mixing 80wt% LNMO, 10wt% SP, and 10% binder in Milli-Q water. The binders were formed by CMC and CP, and their ratio was changed from CMC:CP=10:0, 2:8, 4:6, 6:4, 8:2, 0:10, which were named as CP0, CP2, CP4, CP6, CP8, and CP10. The slurries were coated on Al foils with a doctor-blade and dried at 60 °C. After cutting into 1cm disks, they were dried under vacuum at 120 °C for overnight.

Thermal characterization of DES

Differential scanning calorimetry (DSC) was conducted using a DSC 821 instrument from Mettler-Toledo under a nitrogen flow. The sample was initially cooled from room temperature to −120 °C at a cooling rate of −10 °C min^{-1}, followed by isothermal hold at −120 °C for 5 minutes. Subsequently, a heating scan was recorded from −120 °C to 120 °C at a heating rate of 10 °C min^{-1}.

Spectroscopic characterization

Fourier Transform - Infrared Spectroscopy (FT-IR) was performed using a Nicolet 6700 FT-IR Spectrometer (Thermo Fisher Scientific) employing KBr pellets as a sample medium. A total of 64 scans was performed at a resolution of 4 cm^{-1}, with the resulting data presented as absorption frequencies in units of cm^{-1}.

Raman spectroscopy was carried out using a DILOR LabRam confocal micro-Raman with a He−Ne laser source at 632.7 nm. The Raman energy shift was calibrated using a Si wafer. The spectra were recorded in the vibrational frequencies from 200 to 3000 cm^{-1} with the exposure time of 10 seconds and the accumulation number of 4.

X-ray diffraction (XRD) pattern was recorded using a Rigaku d-max Ultima+diffractometer equipped with a CuKα source from 15° to 80° at the speed of 1° min^{-1}.

Electrochemical characterization

A CR2032 coin cell configuration was utilized. The prepared electrodes based on HC and LNMO were combined with Li-metal anodes and LP30 electrolytes. The prepared cells were subjected to galvanostatic cyclation in a potential range of 0.05 – 2 V vs Li^+/Li at C/10 (1C = 372mA g^{-1}) for 200 cycles in the case of HC. The cells with LNMO were tested in a potential range of 3 – 5 V vs Li^+/Li at 1C for 200 cycles in the case of long-term cycling and at 0.2C, 0.5C, 1C, 2C, and 0.2C, 10 cycles for each C-rate, in the case of rate capability evaluation. Considering the nominal capacity reported by the supplier, 1C was equivalent to 130 mA g^{-1}.

Results and discussion

Development of DES and its use for biomass extraction

For the extraction of CP and LP, a series of DES was prepared following a previously established protocol reported in the literature [36]. The combinations of HBA and HBD are summarized in Table 1, along with their glass transition temperature (T_g) as determined by DSC analysis (thermograms are provided in Figure S1). All the prepared mixtures exhibited a T_g below 0 °C and can therefore be classified as LTTMs, which is considered as a subclass of DESs as explained above [24,37].

Table 1. A series of DESs prepared for the extraction of CP and LP with their T_g.

Samples	Molar Ratio	T_g (°C)
ChCl:resorinol	1:2	-72.23
ChCl:4-methoxypheniol	1:2	-69.74
ChCl:2-methoxyphenol	1:2	-62.89
ChCl:pyrogallol	1:1	T_{g1}= -64.03 / T_{g2}= -51.62

Subsequently, biomass extraction was carried out by using LTTMs. Parameters such as solvent composition, biomass-to-solvent weight ratio, dissolution time and temperature, and the use of an additive (5% H_3PO_3 solution in this case) were systematically evaluated based on the weight of undissolved biomass. Among

examined systems, the most promising one, balancing dissolution efficiency with the mild reaction parameters (i.e., temperature, acid concentration, and reaction time), was identified as ChCl:resorcinol at a 1:2 molar ratio.

By employing the most effective solvent, ChCl:resorcinol at a 1:2, an extraction procedure for CP and LP was established, and the optimized procedure is schematically depicted in Figure 1. Almost complete dissolution of pistachio shell powder was achieved by stirring at 100 °C for 72 hours. This treatment temperature is substantially lower than that of widely used industrial methods including steam explosion. A 1 M aqueous solution of NaOH was added to precipitate CP, followed by washing. The supernatant was neutralized with 1 M HCl, which was then diluted with chilled water to initiate LP flocculation. This precipitate exhibited partial solubility in water at ambient temperature, indicating lignin depolymerisation during the extraction process, as supported by previous experiments reported in the literature [36]. Alternatively, it is possible that only low-molecular-weight lignin was extracted while lignin with higher molecular weight or cross-linked structures might remain insoluble during the pistachio powder dissolution.

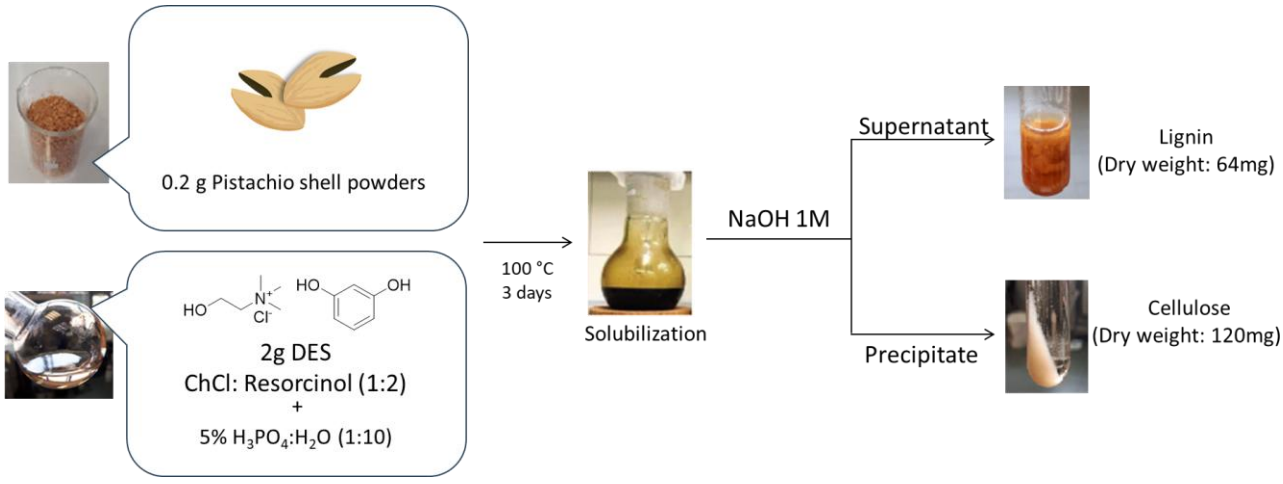

Figure 1. Schematic illustration of CP and LP extraction from pistachio shell powders using DES.

FT-IR characterization of CP and LP

FT-IR spectroscopy was performed to rapidly identify the extracted materials. A shown in Figure 2 (a), the extracted LP exhibited the following diagnostic signals: a broad absorption band at 3400 cm^{-1} attributable to O–H stretching vibrations, two signals at 1601 and 1473 cm^{-1} corresponding to aromatic ring bending modes, various bands with different peak intensities from 1300 to 1000 cm^{-1} arising from various stretching vibrations such as C–O, C–H and C=O [38], and two signals at 960 and 776 cm^{-1} indicative of C–H out-of-plane vibrations [39].

The extracted CP exhibits signal patterns similar to those of commercially available cellulose, AVICEL PH101. The main diagnostic signals were: a band at 3405 cm^{-1} attributable to O-H stretching vibrations, a band at 2987 cm^{-1} attributable to stretching C-H, a signal around 1640 cm^{-1} indicating the O-H bending of adsorbed water, and three characteristic signals for the pyranose ring at 1161, 1114, and 1059 cm^{-1} [40–42]. These results confirm a successful extraction of cellulose and lignin from pistachio shell powders.

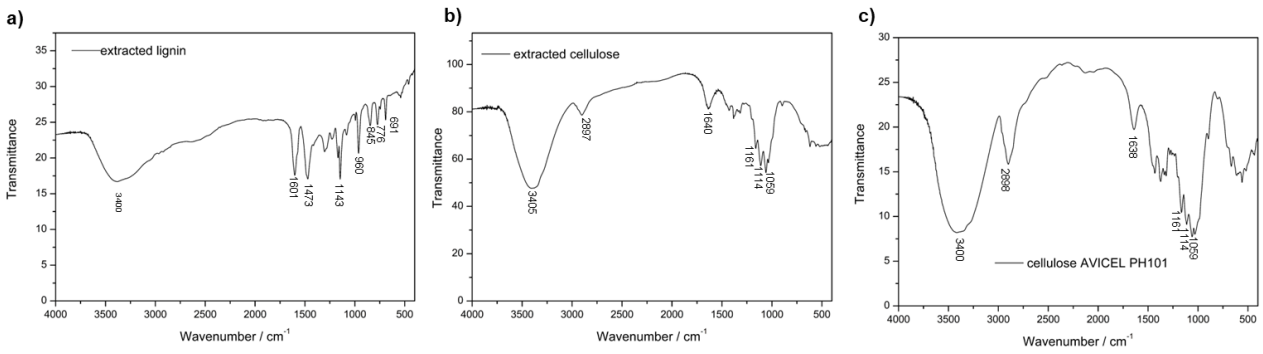

Figure 2. FT-IR spectra of (a) LP, (b) CP, and (c)AVICEL as a reference for CP.

Fundamental characterization of HC synthesized from biomass

Figure 3 (a) summarizes the XRD pattern of LSE before and after pyrolysis, demonstrating the transformation of lignin into HC. In both samples, the broad diffraction patterns can be observed, arising from the amorphous character of materials. For HC, two broad patterns at around 23° and 43° correspond to the crystallographic planes (002) and (100) of carbon materials, respectively. In addition, there are sharp signals at 23.7°, 26.4°, and 32.0° in the pristine LSE, and at 27.6° and 29.3° in the as-made HC. From EDS analysis reported in the supplementary information (Figure S2), the presence of Na, Si, and Ca can be confirmed in LSE, impurity arising from the extraction procedure of LSE or a preexisting contamination in the biomass. Since the peaks of NaOH, Na_2CO_3, NaO_2 are not present in the XRD pattern, Na-related products are expected to present in an amorphous state. The sharp signals in LSE can thus be attributed to $Ca(OH)_2$ and SiO_2, and those in HC can be assigned to $CaCO_3$. The signals of $CaCO_3$ are visible also in the spectrum of purified HC.

As can be seen in Figure 3 (b), Raman spectra of HC exhibit characteristic D and G bands at 1343 and 1584 cm^{-1}, respectively. The former represents the A_{1g} vibration mode of sp^2 carbon rings caused by defects, while the latter corresponds to E_{2g} vibration mode of sp^2 carbon atoms [43]. The relative intensity ratio of the D to G bands (I_D/I_G) is 1.4 and 1.2 for HC before and after purification. The lower I_D/I_G ratio observed after purification suggests a reduction in structural disorder or defects. This may be due to the partial loss of highly disordered, low-density carbon species during the washing process. Specifically, purified HC was recovered from water by centrifugation after sonication, and this step may not be effective in precipitating all

low-density amorphous particles. As a result, the recovered sample may be slightly enriched in more graphitic, higher-density carbon domains, leading to a lower observed I_D/I_G ratio.

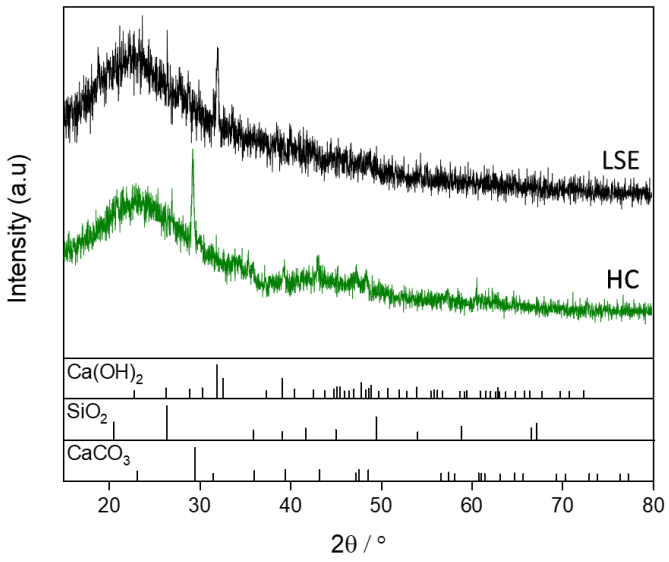

(a)

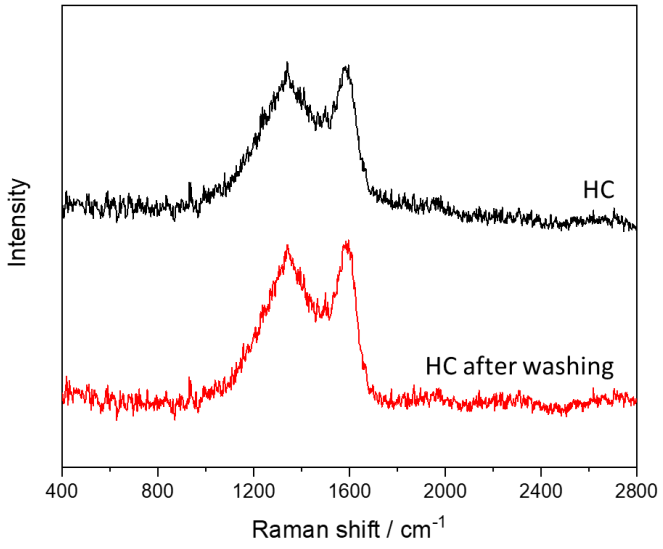

(b)

Figure 3. (a) XRD pattern of LP and as-made HC, reported with reference spectra $Ca(OH)_2$ (PDF#50-0008), SiO_2 (PDF#12-0708), and $CaCO_3$ (PDF#05-0586). (b) Raman spectra of HC before and after washing.

Cell performance of HC synthesized from biomass

Figure 4 demonstrates specific capacity of Li metal cells in which HC is an active material in the counter electrode. The voltage profiles and differential capacity (dQ/dV) curves for 1st and 2nd cycles are provided in the Supporting Information (Figure S3). In both cases, purified HC exhibits better performances compared to as-made HC. As can be seen in Figure 4, capacity values decrease rapidly in the beginning, accompanied by low Coulombic efficiency values, and they stabilize after approximately 25 cycles. The initial low Coulombic efficiency is attributed to the formation of the solid electrolyte interphase (SEI) on the HC surface [44]. When PVdF is used as the binder, SEI formation is observed at 0.7 V vs. Li^+/Li for pristine HC and at 0.8 V vs. Li^+/Li for purified HC, as shown in the dQ/dV curves (Figure S3). In contrast, the SEI formation voltage shifts to a lower value when CMC is used as the binder. SEI formation is an irreversible process, and the corresponding signals disappear after the first cycle. Consequently, in successive cycles, the voltage profile exclusively reflects the lithiation/de-lithiation behavior of HC, which is characterized by a slope pattern.

The charge capacity values at the 50th cycle reach 320.4 and 216.2 mAh g^{-1} for pristine and purified HC with PVdF binder and 346.4 and 285.1 mAh g^{-1} for those with CMC binder. The enhanced capacity for the cell with CMC is due to more homogeneous distribution of the active material, as already reported in the literature for other carbon-based electrodes [45,46]. In addition, CMC is a promising binder particularly for carbon-based anodes because of its unique hydrophobic-hydrophilic balance, improving electrode integrity [47]. At the 200th cycle, capacity retention is found to be 93.6 and 97.3% for the HC-PVdF samples and 92.9 and 85.8 % for the HC-CMC, purified and non-purified, respectively, compared to the 50th cycle. It seems the

impurities in HC have the effect of capacity reduction from the beginning of cycling with PVdF, while this negative effect is somehow mediated in the beginning with the presence of CMC. Better capacity values are observed when CMC is the binder, while better capacity retentions are confirmed when PVdF is the binder.

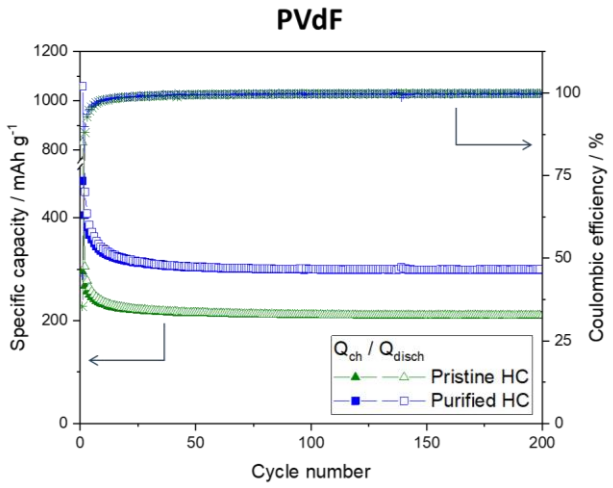

(a)

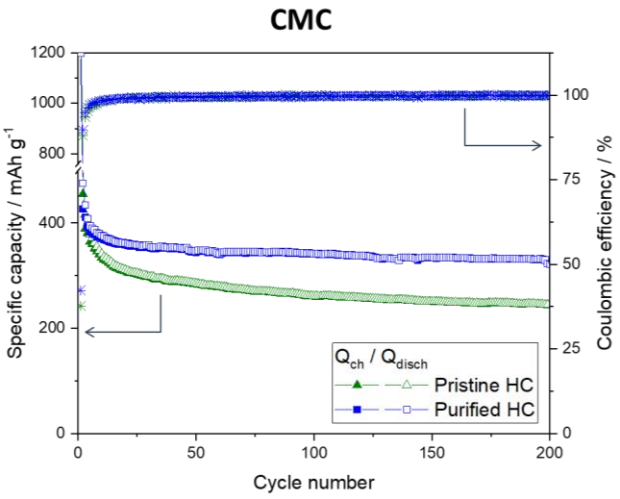

(b)

Figure 4. Specific capacity (Q) of Li||HC cell in which (a) PVdF and (b) CMC is used as the binder, cycled at C/10.

Cell performance of LNMO cathode with cellulose-based binders

Figure 5 summarizes the rate capability of Li-metal cells employing LNMO cathodes with different binder ratios of CP and CMC. With the exception of the electrodes with larger ratios of CP, specifically CP8 and CP10, the electrodes exhibited good rate capabilities, *i.e.*, a capacity value over 100 mAh g^{-1} regardless the C-rate. When the cycling speed is 2C, specific discharge capacities of the cells decrease with increasing amount of CP, suggesting CMC is a better binder for higher speed cycling. Figure S4 exhibits impedance spectra of the cells after the rate capability analysis and Table S1 summarizes bulk and interfacial resistance values (R_{bulk} and R_{int}) calculated from the spectra. The R_{bulk} values are higher for CP0 and CP2, while they are similar among CP4, 6, 8, and 10. With respect to R_{int}, which is derived from the diameter of the semicircle appearing in each impedance spectrum, calculated by fitting so that it estimates the major axis of an ellipse, low values are observed for CP2 and CP4, and the value increases by increasing the concentration of CP over CMC. This would be the reason for the lower capacity at higher C-rate values of the cell having CP as a major component of the binder. In the case of CP0, in which CP is absent, its R_{bulk} and R_{int} are substantially high, but the overpotential of the cell is low compared to the cells containing CP (see Figure S5 for voltage profiles at 2C). From the voltage profile, it also can be noticed that the voltage plateau at ca. 4.0 V vs Li^+/Li is larger for CP0 compared to other cells, which is related to $Mn^{3+/4+}$ redox observed for disordered LNMO [48]. Enhanced $Mn^{3+/4+}$ redox has already been observed when CMC-based binder is used [49].

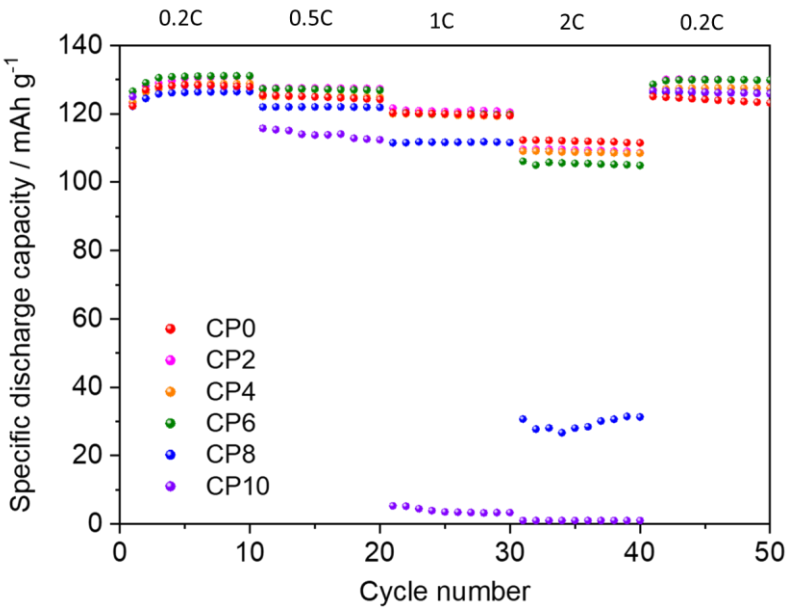

Figure 5. Rate capability analysis at 0.2C, 0.5C, 1C, 2C, and 0.2C of LNMO cathodes with different binder composition (CMC:CP=10:0, 2:8, 4:6, 6:4, 8:2, 0:10 named as CP0, CP2, CP4, CP6, CP8, and CP10).

The clear trend of capacity increase being inversely related to the ratio of CMC over CP, which can be observed at 2C, is not observed when the C-rate is lower than 1C. When the specific capacities of the 10th and 50th cycles are compared, both of which are cycled at 0.2C, the best capacity retention is achieved by CP8 (99.6%) and decreases as follows: CP2 (99.1%), CP6 (99.1%), CP4 (99.0%) > CP10 (98.5%) > CMC (97.6%). This suggests that the addition of CP to CMC has an advantageous effect on long-term cycling. To confirm this, long-term stability was analyzed as shown in Figure 6. When CMC is absent (CP10), the cell exhibits low and non-constant capacity values over 200 cycles. In all cases, capacity value increases in the first 10 cycles, and at the 10th cycle, a better specific discharge capacity is found for the cell with a higher amount of CMC which is consistent with the results of the rate capability analysis. Capacity retention values at the 200 cycle with respect to that of the

10^{th} cycle is 78.6, 94.6, 94.6, 94.5, and 99.5 % for CP0, CP2, CP4, CP6, and CP8. Therefore, the use of CP as the binder is confirmed to be favorable for long-term cycling. Figure S6 reports dQ/dV curves of cells with varying CP content in binder (CP0–CP10), comparing the 10^{th} and 200^{th} cycles. In all samples, two distinct oxidation peaks are observed: one at around 4.1 V vs Li^+/Li for Mn^{3+}/Mn^{4+} and another at around 4.8 V vs Li^+/Li attributed to the multiple-step oxidation of nickel (Ni^{2+}/Ni^{3+} and Ni^{3+}/Ni^{4+}). The oxidation voltage of nickel tends to increase when the CP concentration is high. In contrast, its voltage gap between the 10^{th} and 200^{th} cycles ($\Delta V_{10th-200th}$) decreases with increasing CP content. For example, CP0 and CP2 show relatively large $\Delta V_{10th-200th}$ of 29 mV and 40 mV, respectively, indicating greater overpotential growth. This trend suggests that the inclusion of CP suppresses the increase in overpotential upon long-term cycling.

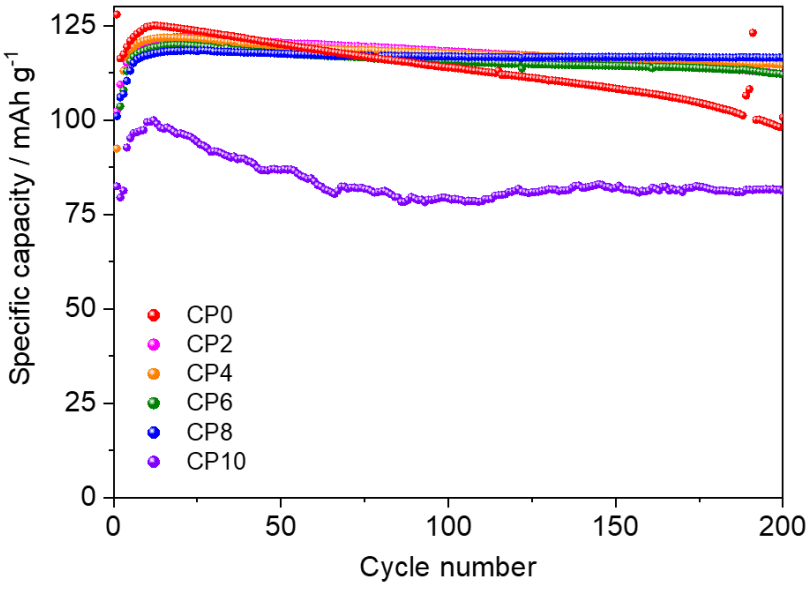

Figure 6. Long-term cycling at 1C of LNMO cathodes with different binder composition (CMC:CP=10:0, 2:8, 4:6, 6:4, 8:2, 0:10 named as CP0, CP2, CP4, CP6, CP8, and CP10).

Conclusion

The extraction procedure of CP and LP from pistachio shells was developed by using DES as the green solvent. Along with LSE, these extracted materials were used for the development of battery components. HC prepared from LSE was examined as the active material in Li-metal batteries. Specific capacities of the 50th charge are 320.4 and 216.2 mAh g^{-1} for the HC-PVdF samples and 346.4 and 285.1 mAh g^{-1} for the HC-CMC samples, purified and non-purified, respectively, and at the 200th cycle, capacity retention was found to be 93.6 and 97.3% for the former couple and 92.9 and 85.8 % for the latter couple. On the other hand, CP was developed as the binder for the LNMO cathode, as the substitute of CMC binder. The use of CMC was found to be favorable for a high-speed cycling, while that of CP was favorable for long-term cycling.

Acknowledgements

The project is financially supported by Progetto Eco-Rete Green within the framework of Progetti Strategici 2019 - POR FESR Lazio 2014-2020. A.T. acknowledges the financial support from the Sapienza University of Rome for the Ateneo project 2022 for “Naturally Derived Battery Components for Safe, Stable, and Sustainable Energy Storage System (3S-ESS)” (protocol no. RP1221816C3CC15E). The LSE was kindly provided by Dr. Francesco Zimbardi at the Trisaia Research Centre, ENEA.

Reference

[1] A. Colmenar-Santos, A.-M. Muñoz-Gómez, E. Rosales-Asensio, Á. López-Rey, Electric vehicle charging strategy to support renewable energy sources in Europe 2050 low-carbon scenario, Energy

183 (2019) 61–74. https://doi.org/10.1016/j.energy.2019.06.118.

[2] M. Titirici, P. Johansson, M. Crespo Ribadeneyra, H. Au, A. Innocenti, S. Passerini, E. Petavratzi, P. Lusty, A.A. Tidblad, A.J. Naylor, R. Younesi, Y.A. Chart, J. Aspinall, M. Pasta, J. Orive, L.M. Babulal, M. Reynaud, K.G. Latham, T. Hosaka, S. Komaba, J. Bitenc, A. Ponrouch, H. Zhang, M. Armand, R. Kerr, P.C. Howlett, M. Forsyth, J. Brown, A. Grimaud, M. Vilkman, K.B. Dermenci, S. Mousavihashemi, M. Berecibar, J.E. Marshall, C.R. McElroy, E. Kendrick, T. Safdar, C. Huang, F.M. Zanotto, J.F. Troncoso, D.Z. Dominguez, M. Alabdali, U. Vijay, A.A. Franco, S. Pazhaniswamy, P.S. Grant, S. López Guzman, M. Fehse, M. Galceran, N. Antuñano, 2024 roadmap for sustainable batteries, Journal of Physics: Energy 6 (2024) 041502. https://doi.org/10.1088/2515-7655/ad6bc0.

[3] S. Dühnen, J. Betz, M. Kolek, R. Schmuch, M. Winter, T. Placke, Toward Green Battery Cells: Perspective on Materials and Technologies, Small Methods 4 (2020). https://doi.org/10.1002/smtd.202000039.

[4] V.G. Pol, Lithium-Ion Battery Critical Materials Sustainability, ACS Energy Lett 10 (2025) 2553–2558. https://doi.org/10.1021/acsenergylett.5c01018.

[5] P. Molaiyan, S. Bhattacharyya, G.S. dos Reis, R. Sliz, A. Paolella, U. Lassi, Towards greener batteries: sustainable components and materials for next-generation batteries, Green Chemistry 26 (2024) 7508–7531. https://doi.org/10.1039/D3GC05027K.

[6] E. Lewicka, K. Guzik, K. Galos, On the Possibilities of Critical Raw Materials Production from the EU's Primary Sources, Resources 10 (2021) 50. https://doi.org/10.3390/resources10050050.

[7] H. He, R. Zhang, P. Zhang, P. Wang, N. Chen, B. Qian, L. Zhang, J. Yu, B. Dai, Functional Carbon from Nature: Biomass - Derived Carbon Materials and the Recent Progress of Their Applications, Advanced Science 10 (2023). https://doi.org/10.1002/advs.202205557.

[8] X. Casas, M. Niederberger, E. Lizundia, A Sodium-Ion Battery Separator with Reversible Voltage Response Based on Water-Soluble Cellulose Derivatives, ACS Appl Mater Interfaces (2020) acsami.0c05262. https://doi.org/10.1021/acsami.0c05262.

[9] M. Binder, E. Keller, D. Bresser, Realization of high mass loading LiNi0.5Mn1.5O4 Li-ion cathodes using water-soluble carrageenan as binder, J Power Sources 603 (2024) 234487. https://doi.org/10.1016/j.jpowsour.2024.234487.

[10] D. Bresser, D. Buchholz, A. Moretti, A. Varzi, S. Passerini, Alternative binders for sustainable electrochemical energy storage – the transition to aqueous electrode processing and bio-derived polymers, Energy Environ Sci 11 (2018) 3096–3127. https://doi.org/10.1039/C8EE00640G.

[11] R. Xu, V. Pamidi, Y. Tang, S. Fuchs, H.S. Stein, B. Dasari, Z. Zhao - Karger, S. Behara, Y. Hu, S. Trivedi, M. Anji Reddy, P. Barpanda, M. Fichtner, Greener, Safer and Better Performing Aqueous Binder for Positive Electrode Manufacturing of Sodium Ion Batteries, ChemSusChem 17 (2024). https://doi.org/10.1002/cssc.202301154.

[12] S.S. Varshni, A.V. Murugan, Enhanced Cathode–Electrolyte Interfaces Formation via Lithium-Phytate Chelation for an Aqueous-Processed $LiNi_{0.7}Mn_{0.25}Al_{0.05}O_2$ High-Voltage Cathode, Energy & Fuels 39 (2025) 11981–11994. https://doi.org/10.1021/acs.energyfuels.5c01251.

[13] A.C. Rolandi, I. de Meatza, N. Casado, M. Forsyth, D. Mecerreyes, C. Pozo-Gonzalo, Unlocking sustainable power: advances in aqueous processing and water-soluble binders for NMC cathodes in high-voltage Li-ion batteries, RSC Sustainability 2 (2024) 2125–2149. https://doi.org/10.1039/D4SU00098F.

[14] I. Dienwiebel, M. Diehl, B. Heidrich, X. Yang, M. Winter, M. Börner, Enabling Aqueous Processing for $LiNi_{0.5}Mn_{1.5}O_4$ - Based Positive Electrodes in Lithium - Ion Batteries by Applying Lithium - Based Processing Additives, Advanced Energy and Sustainability Research 2 (2021). https://doi.org/10.1002/aesr.202100075.

[15] S. Tagliaferri, L. Gaspard, H. Au, C. Mattevi, M.-M. Titirici, M. Crespo-Ribadeneyra, Nature-inspired batteries: from biomaterials to biomimetic design strategies, Green Chemistry 26 (2024) 6944–6958. https://doi.org/10.1039/D4GC00638K.

[16] S.K. Saju, S. Chattopadhyay, J. Xu, S. Alhashim, A. Pramanik, P.M. Ajayan, Hard carbon anode for lithium-, sodium-, and potassium-ion batteries: Advancement and future perspective, Cell Rep Phys Sci 5 (2024) 101851. https://doi.org/10.1016/j.xcrp.2024.101851.

[17] Y. Wang, J. Yang, G. Duan, R. Yu, X. Han, C. Zhang, J. Han, Q. Fu, H. Yang, S. He, S. Jiang, The role of carbonization temperature and amorphous components for the design and optimization of wood-based hard carbon thick electrodes in lithium-ion batteries, Ind Crops Prod 227 (2025) 120764. https://doi.org/10.1016/j.indcrop.2025.120764.

[18] G. Zhang, C. Chen, C. Xu, J. Li, H. Ye, A. Wang, X. Cao, K. Sun, J. Jiang, Unraveling the Microcrystalline Carbon Evolution Mechanism of Biomass-Derived Hard Carbon for Sodium-Ion Batteries, Energy & Fuels 38 (2024) 8326–8336. https://doi.org/10.1021/acs.energyfuels.4c00823.

[19] D. Alvira, D. Antorán, H. Darjazi, G.A. Elia, C. Gerbaldi, V. Sebastian, J.J. Manyà, High performing and sustainable hard carbons for Na-ion batteries through acid-catalysed hydrothermal carbonisation of vine shoots, J Mater Chem A Mater 13 (2025) 2730–2741. https://doi.org/10.1039/D4TA07393B.

[20] J. Wang, J. Zhao, X. He, Y. Qiao, L. Li, S.-L. Chou, Hard carbon derived from hazelnut shell with facile HCl treatment as high-initial-coulombic-efficiency anode for sodium ion batteries, Sustainable Materials and Technologies 33 (2022) e00446. https://doi.org/10.1016/j.susmat.2022.e00446.

[21] S. Larsson, E. Palmqvist, B. Hahn-Hägerdal, C. Tengborg, K. Stenberg, G. Zacchi, N.-O. Nilvebrant, The generation of fermentation inhibitors during dilute acid hydrolysis of softwood, Enzyme Microb Technol 24 (1999) 151–159. https://doi.org/10.1016/S0141-0229(98)00101-X.

[22] Y. Zhao, Y. Wang, J.Y. Zhu, A. Ragauskas, Y. Deng, Enhanced enzymatic hydrolysis of spruce by alkaline pretreatment at low temperature, Biotechnol Bioeng 99 (2008) 1320–1328. https://doi.org/10.1002/bit.21712.

[23] M. Francisco, A. van den Bruinhorst, M.C. Kroon, Low - Transition - Temperature Mixtures (LTTMs): A New Generation of Designer Solvents, Angewandte Chemie International Edition 52 (2013) 3074–3085. https://doi.org/10.1002/anie.201207548.

[24] J.L. Wong, S.N.B.A. Khadaroo, J.L.Y. Cheng, J.J. Chew, D.S. Khaerudini, J. Sunarso, Green solvent

for lignocellulosic biomass pretreatment: An overview of the performance of low transition temperature mixtures for enhanced bio-conversion, Next Materials 1 (2023) 100012. https://doi.org/10.1016/j.nxmate.2023.100012.

[25] M. Palluzzi, A. Tsurumaki, H. Adenusi, M.A. Navarra, S. Passerini, Ionic liquids and their derivatives for lithium batteries: role, design strategy, and perspectives, Energy Materials 3 (2023) 300049. https://doi.org/10.20517/energymater.2023.48.

[26] C.E. Okonkwo, S.Z. Hussain, S. Manzoor, B. Naseer, A.E. Taiwo, M. Ayyash, A.H. Al-Marzouqi, A. Kamal-Eldin, A comprehensive review on the use of deep eutectic solvents for biomass processing, and the synergistic coupling with physical technology and biological method, Bioresour Technol Rep 23 (2023) 101577. https://doi.org/10.1016/j.biteb.2023.101577.

[27] M. Zdanowicz, K. Wilpiszewska, T. Spychaj, Deep eutectic solvents for polysaccharides processing. A review, Carbohydr Polym 200 (2018) 361–380. https://doi.org/10.1016/j.carbpol.2018.07.078.

[28] D.J.G.P. van Osch, L.J.B.M. Kollau, A. van den Bruinhorst, S. Asikainen, M.A.A. Rocha, M.C. Kroon, Ionic liquids and deep eutectic solvents for lignocellulosic biomass fractionation, Physical Chemistry Chemical Physics 19 (2017) 2636–2665. https://doi.org/10.1039/C6CP07499E.

[29] Y.-L. Loow, E.K. New, G.H. Yang, L.Y. Ang, L.Y.W. Foo, T.Y. Wu, Potential use of deep eutectic solvents to facilitate lignocellulosic biomass utilization and conversion, Cellulose 24 (2017) 3591–3618. https://doi.org/10.1007/s10570-017-1358-y.

[30] W. Wang, D.-J. Lee, Lignocellulosic biomass pretreatment by deep eutectic solvents on lignin extraction and saccharification enhancement: A review, Bioresour Technol 339 (2021) 125587. https://doi.org/10.1016/j.biortech.2021.125587.

[31] K. Kohli, S. Katuwal, A. Biswas, B.K. Sharma, Effective delignification of lignocellulosic biomass by microwave assisted deep eutectic solvents, Bioresour Technol 303 (2020) 122897. https://doi.org/10.1016/j.biortech.2020.122897.

[32] L. Zhang, C. Zhang, Y. Ma, X. Zhao, X. Zhang, Lignocellulose pretreatment by Deep eutectic solvent and water binary system for enhancement of lignin extraction and cellulose saccharification, Ind Crops Prod 211 (2024) 118257. https://doi.org/10.1016/j.indcrop.2024.118257.

[33] Z. Chen, X. Bai, L. A, C. Wan, High-Solid Lignocellulose Processing Enabled by Natural Deep Eutectic Solvent for Lignin Extraction and Industrially Relevant Production of Renewable Chemicals, ACS Sustain Chem Eng 6 (2018) 12205–12216. https://doi.org/10.1021/acssuschemeng.8b02541.

[34] C. Bonini, M. D'Auria, G. Mauriello, R. Pucciariello, R. Teghil, D. Tofani, L. Viggiani, D. Viggiano, F. Zimbardi, Graft copolymers of lignin from straw with 1-ethenylbenzene: Synthesis and characterization, J Appl Polym Sci 79 (2001) 72–79. https://doi.org/10.1002/1097-4628(20010103)79:1<72::AID-APP80>3.0.CO;2-F.

[35] E. Unur, S. Brutti, S. Panero, B. Scrosati, Nanoporous carbons from hydrothermally treated biomass as anode materials for lithium ion batteries, Microporous and Mesoporous Materials 174 (2013) 25–33. https://doi.org/10.1016/j.micromeso.2013.02.032.

[36] P. Li, Z. Zhang, X. Zhang, K. Li, Y. Jin, W. Wu, DES: their effect on lignin and recycling performance,

RSC Adv 13 (2023) 3241–3254. https://doi.org/10.1039/D2RA06033G.

[37] P. Tomai, A. Lippiello, P. D'Angelo, I. Persson, A. Martinelli, V. Di Lisio, R. Curini, C. Fanali, A. Gentili, A low transition temperature mixture for the dispersive liquid-liquid microextraction of pesticides from surface waters, J Chromatogr A 1605 (2019) 360329. https://doi.org/10.1016/j.chroma.2019.06.050.

[38] R.J.A. Gosselink, A. Abächerli, H. Semke, R. Malherbe, P. Käuper, A. Nadif, J.E.G. van Dam, Analytical protocols for characterisation of sulphur-free lignin, Ind Crops Prod 19 (2004) 271–281. https://doi.org/10.1016/j.indcrop.2003.10.008.

[39] C.G. Boeriu, D. Bravo, R.J.A. Gosselink, J.E.G. van Dam, Characterisation of structure-dependent functional properties of lignin with infrared spectroscopy, Ind Crops Prod 20 (2004) 205–218. https://doi.org/10.1016/j.indcrop.2004.04.022.

[40] M.M. Ibrahim, F.A. Agblevor, W.K. El-Zawawy, Isolation and characterization of cellulose and lignin from steam-exploded lignocellulosic biomass, Bioresources 5 (2010) 397–418. https://doi.org/10.15376/biores.5.1.397-418.

[41] W. Chen, H. He, H. Zhu, M. Cheng, Y. Li, S. Wang, Thermo-Responsive Cellulose-Based Material with Switchable Wettability for Controllable Oil/Water Separation, Polymers (Basel) 10 (2018) 592. https://doi.org/10.3390/polym10060592.

[42] S.Y. Oh, D. Il Yoo, Y. Shin, G. Seo, FTIR analysis of cellulose treated with sodium hydroxide and carbon dioxide, Carbohydr Res 340 (2005) 417–428. https://doi.org/10.1016/j.carres.2004.11.027.

[43] Y. Jin, S. Sun, M. Ou, Y. Liu, C. Fan, X. Sun, J. Peng, Y. Li, Y. Qiu, P. Wei, Z. Deng, Y. Xu, J. Han, Y. Huang, High-Performance Hard Carbon Anode: Tunable Local Structures and Sodium Storage Mechanism, ACS Appl Energy Mater 1 (2018) 2295–2305. https://doi.org/10.1021/acsaem.8b00354.

[44] B. Babu, P. Simon, A. Balducci, Fast Charging Materials for High Power Applications, Adv Energy Mater 10 (2020). https://doi.org/10.1002/aenm.202001128.

[45] R. Gond, H.D. Asfaw, O. Hosseinaei, K. Edström, R. Younesi, A.J. Naylor, A Lignosulfonate Binder for Hard Carbon Anodes in Sodium-Ion Batteries: A Comparative Study, ACS Sustain Chem Eng 9 (2021) 12708–12717. https://doi.org/10.1021/acssuschemeng.1c05263.

[46] J. Jiao, C. Yi, X. Qiu, D. Yang, F. Fu, W. Liu, Green biomass: the impact of high-adhesion and well-dispersed binders on the sodium storage performance and interfacial interaction of hard carbon anodes, Green Chemistry 26 (2024) 6643–6655. https://doi.org/10.1039/D4GC00808A.

[47] J. Li, A. Wang, W. Xiang, S. Liu, L. Li, Q. Wu, Y. Liu, Y. Liu, G. Nie, S. Nie, S. Yao, H. Yu, Direct synthesis of a lithium carboxymethyl cellulose binder using wood dissolving pulp for high-performance LiFePO4 cathodes in lithium-ion batteries, Bioresour Technol 401 (2024) 130711. https://doi.org/10.1016/j.biortech.2024.130711.

[48] S. Choi, W. Feng, Y. Xia, Recent Progress of High Voltage Spinel $LiMn_{1.5}Ni_{0.5}O_4$ Cathode Material for Lithium-Ion Battery: Surface Modification, Doping, Electrolyte, and Oxygen Deficiency, ACS Omega 9 (2024) 18688–18708. https://doi.org/10.1021/acsomega.3c09101.

[49] S. Hitomi, K. Kubota, T. Horiba, K. Hida, T. Matsuyama, H. Oji, S. Yasuno, S. Komaba, Application of Acrylic - Rubber - Based Latex Binder to High - Voltage Spinel Electrodes of Lithium - Ion Batteries, ChemElectroChem 6 (2019) 5070–5079. https://doi.org/10.1002/celc.201901227.